HHS Public Access

Author manuscript

Nat Biomed Eng. Author manuscript; available in PMC 2018 September 07.

Published in final edited form as:

Nat Biomed Eng. 2018 March ; 2(3): 183–194.

Cell-type-specific brain methylomes profiled via ultralow-input microfluidics

Sai Ma[1], **Mario de la Fuente Revenga**[2], **Zhixiong Sun**[3], **Chen Sun**[1], **Travis W. Murphy**[4], **Hehuang Xie**[5,6,3], **Javier González-Maeso**[2], and **Chang Lu**[4,*]

[1]Department of Biomedical Engineering and Mechanics, Virginia Tech, Blacksburg, VA 24061, USA

[2]Department of Physiology and Biophysics, Virginia Commonwealth University School of Medicine, Richmond, VA 23298, USA

[3]Department of Biological Sciences, Virginia Tech, Blacksburg, VA 24061, USA

[4]Department of Chemical Engineering, Virginia Tech, Blacksburg, VA 24061, USA

[5]Biocomplexity Institute of Virginia Tech, Blacksburg, VA 24061, USA

[6]Department of Biomedical Sciences and Pathobiology, Virginia-Maryland College of Veterinary Medicine, Blacksburg, VA 24061, USA

Abstract

Methylomic analyses typically require substantial amounts of DNA, thus hindering studies involving scarce samples. Here, we show that microfluidic diffusion-based reduced representative bisulfite sequencing (MID-RRBS) permits high-quality methylomic profiling with nanogram-to-single-cell quantities of starting DNA. We used the microfluidic device, which allows for efficient bisulfite conversion with high DNA recovery, to analyse genome-wide DNA methylation in cell nuclei isolated from mouse brains and sorted into NeuN+ (primarily neuronal) and NeuN− (primarily glial) fractions, and to establish cell-type-specific methylomes. Genome-wide methylation and methylation in low-CpG-density promoter regions showed distinct patterns for NeuN+ and NeuN− fractions from the mouse cerebellum. The identification of substantial variations in the methylomic landscapes of the NeuN+ fraction of the frontal cortex of mice chronically treated with an atypical antipsychotic drug suggests that this technology can be broadly used for cell-type-specific drug profiling and for the study of drug-methylome interactions.

*Corresponding author (C.L.): changlu@vt.edu.

Author contributions

C.L. and S.M. designed the microfluidic device. S.M. and C.L. developed the MID-RRBS protocol. C.L. supervised the research. C.L., S.M., J.G.-M., and H.X. designed the biological experiments. S.M. conducted experiments to generate MID-RRBS and mRNA-seq data on the cell/brain samples and performed data analysis. M.F.R. performed the clozapine treatment and sample collection. Z.S. helped with the device characterization. C.S. and T.W.M. helped with device fabrication and setup. C.L. and S.M. wrote the manuscript. All authors proofread the manuscript and provided comments.

Competing interests

The authors declare no competing financial interests.

Introduction

DNA methylation patterns in the genome (i.e. DNA methylomes) critically affect gene activities as a part of overall epigenetic regulatory program during normal development and disease processes. CpG dinucleotides are important targets for methylation (mCG). Hypermethylation on CpG island (CGI) promoters is a common mechanism for gene silencing and an epigenetic feature for many types of human cancers [1]. Both mCG [2,3] and non-CG methylation (mCH, where H = A, C, or T) [4,5] are critically involved in human neuronal genome and their dynamics play critical roles in mammalian brain development. There have been a number of genome-wide technologies for profiling DNA methylomes developed over the years. Whole-genome bisulfite sequencing (WGBS) is generally considered the gold standard for DNA methylation analyses [6,7]. Bisulfite treatment converts cytosine residues to uracils, with 5-methylcytosine residues unaffected. Combined with high-throughput sequencing, the approach generates methylomic profiles with single-nucleotide resolution. Despite of the high resolution, the cost associated with deep sequencing required by WGBS (>500 million reads per sample to cover human genome) can be prohibitive. In comparison, enrichment-based technologies reduce the required sequencing depth by enriching methylated DNA fragments based on affinity purifications, at a price of low resolution (100–300 bp) [8,9]. As another cost-effective alternative to WGBS, reduced representative bisulfite sequencing (RRBS) utilizes methylation-insensitive restriction enzyme (MspI) digestion and size selection to enrich a subset of the genome (mostly CpG islands and promoter regions) for analysis while preserving single-nucleotide resolution [10,11].

Prevailing WGBS and RRBS protocols require substantial amounts of genomic DNA. WGBS requires 10 ng to 5 μg input DNA [6,7,12]. RRBS typically requires >300 ng DNA to detect 1.0–2.2 million unique CpGs (≥1× coverage) and merely 0.3–1.0 million CpGs with ≥10× coverage in human genome. Recent efforts on low-input RRBS lowered the starting DNA amount to 30 ng with compromised CpG recovery (< 1 million unique CpGs) [11]. Single-cell RRBS [13] and WGBS [14–16] were also demonstrated recently. These single-cell assays cover only a small fraction of the genome [13–16]. Thus when cell-to-cell variability is not the focus of a study, low-input methods (using a low number of cells) offer much higher breath of coverage for the genome and distinct advantages over their single-cell counterparts. These low-input methods are useful for establishing reference epigenomes using scarce primary tissues and profiling patient materials for treatment stratification.

Microfluidics has proven to be a powerful platform for genomic and transcriptomic analysis of cells [17–21]. Microfluidic devices have also been applied to study epigenomics recently [22,23]. Bisulfite conversion was implemented in both channel [24] and droplet [25] formats for examining DNA methylation at single loci. Here we demonstrate a microfluidic technology, referred to as MIcrofluidic Diffusion-based RRBS (MID-RRBS), for low-input assays (down to 0.3 ng DNA and single cells) with high bisulfite conversion efficiency and high coverage of CpGs. We used a diffusion-based reagent swapping approach for multi-step treatment of DNA on the microfluidic system. Our protocol preserved substantially more amplifiable DNA than conventional bisulfite treatment [10,26–28] while achieving high

conversion rate. We mapped methylomes of a cell line (GM 12878), NeuN+ (primarily neuronal) and NeuN− (primarily glial) fractions isolated from mouse brains. Our protocol yielded data that were heavy in CpGs of high coverage (2.0–2.6 million CpGs with ≥1×, 1.3–1.8 million CpGs with ≥10× coverage with 0.3 to 10 ng starting DNA, respectively). We also demonstrated the capability of MID-RRBS for parallel processing of multiple samples and single cell profiling. MID-RRBS technology allowed differentiation of methylomic landscapes of NeuN+ and NeuN− fractions from mouse cerebellum, generating insights into cell-type-specific features. Finally, we discovered changes in the mouse frontal cortex NeuN + methylome associated with chronic administration of an atypical antipsychotic drug clozapine, establishing the feasibility for applying the technology to study drug-methylome interactions relevant to drug development.

Results

Device and protocol for MID-RRBS

Our microfluidic device consisted of a reaction chamber (~240 nl in volume) connected with two loading chambers (~480 nl each) on both sides (Fig. 1a and Supplementary Fig. 1). The reaction chamber and the loading chambers could be disconnected by actuating a pair of pneumatic valves in between them. We conducted bisulfite conversion using a diffusion-based reagent swapping method. This approach takes advantage of the difference in the diffusivities of DNA and small molecules. DNA molecules of substantial sizes have much lower diffusivity than small-molecule reagents involved in DNA treatment. When material exchange occurs by diffusion for a short period, DNA loss from the reaction chamber is minimal, whereas a small-molecule reagent in the same chamber gets released (into the loading chambers) and replaced by another small-molecule reagent needed for the next step almost completely. Although we applied similar principle to process large DNA fragments (~50 kb) in previous work [29], treating DNA fragments of several hundred base pairs, which are relevant to next-generation sequencing, remains challenging. In our process (Fig. 1b), a genomic DNA sample (160–360 bp) was loaded into the reaction chamber and a bisulfite conversion buffer was loaded in the loading chambers, while the valves between the chambers were closed. The dosing of bisulfite mix into the reaction chamber then occurred by opening the valves and allowing diffusion under concentration gradients (in 3 periods of 10 min each, with the loading chambers replenished with fresh bisulfite mix after each period). The diffusivity of DNA fragments (e.g. 2×10^{-11} m^2/s for ~250 bp DNA) differs from those of small-molecule reagents (~10^{-9} m^2/s) roughly by 2 orders of magnitude. Thus the bulk of the DNA molecules (93% estimated by COMSOL modeling in Fig. 1c) remained in the reaction chamber, while the small-molecule bisulfite mix filled up the reaction chamber to reach 98% and 97% of the loading concentrations for sodium bisulfite and quinol, respectively (Fig. 1c). After sulphonation of 1 h at 55 °C with all valves closed, using the same diffusion-based swapping scheme, NaOH was loaded into the reaction chamber to replace bisulfite mix for desulphonation. The valves were then closed for 20 min to allow desulphonation to take place in the reaction chamber. DNA was finally eluted out of the device for ethanol precipitation and downstream sequencing. It is worth noting that our process eliminated column-based DNA purification between bisulfite conversion and desulphonation (which may cause loss up to 80–90% of DNA [28]). Small-molecule reagents

in the reaction chamber were effectively removed by the diffusion step after their reactions (e.g. the concentration of sodium bisulfite in the reaction chamber fell to 2% of its original one after three 10-min periods of diffusion, Fig. 1c).

In order to quantify DNA recovery by MID-RRBS technology, we used our device and protocol to process a 272-bp DNA template containing adapters attached to the ends (Supplementary Fig. 2). We measured the amount of DNA recovery using qPCR after MID-bisulfite conversion of various durations. The qPCR assay quantified the amount of DNA with both adapters intact after bisulfite conversion and the results reflected both DNA diffusion out of the reaction chamber during loading and loss in DNA functionality due to bisulfite treatment. We recovered 41.9, 34.5%, and 29.6% of the starting DNA template after our microfluidic bisulfite conversion for 0.5, 1, and 2 h, respectively (Supplementary Fig. 2).

To benchmark performance of MID-RRBS, we used our technology to profile the methylome of GM12878 cells (a lymphoblastoid cell line). We varied the amount of starting genomic DNA in the range of 0.3 to 10 ng. After MspI digestion and adapter ligation, DNA fragments in the range of 160–360 bp (with insert sizes of 40–240 bp) were selected by gel-free size selection (Supplementary Fig. 3) [30]. MID-RRBS was conducted and sequencing data were analyzed. We achieved averagely 99.8 ± 0.1% conversion rates using our protocol (Supplementary Table 1). The detected unique CpGs ranged from 74.5% of theoretical maximum (i.e. 2.07 out of 2.79 million) with 0.3 ng DNA to 92.0% with 10 ng DNA whereas CpGs with ≥10× coverage ranged from 49.7% with 0.3 ng to 63.2% with 10 ng DNA (Fig. 2a). For comparison, we also used a commercial kit from Zymo that was used in a number of recent works [31–33]. The Zymo kit utilizes the same conversion reagents as in MID-RRBS. We applied the kit to produce data using 1 μg and 1 ng DNA samples (Supplementary Table 1). Zymo datasets generated 97.2% and 66.5% unique CpGs using 1 μg and 1 ng samples, respectively. However, Zymo 1 ng datasets generated very few 10× CpGs (averagely 28.9%), compared to MID-RRBS 1 ng and 0.3 ng samples (52.3% and 49.7%, respectively). The MID-RRBS datasets generated 0.050–0.084 million unique CpGs per million trimmed reads with the peak values reached with 1 ng samples (Supplementary Fig. 4). MID-RRBS samples of 10, 3, 1, and 0.3 ng had Pearson coefficients of 0.95, 0.98, 0.96, and 0.84 between replicates, respectively (Fig. 2b). Zymo datasets had Pearson correlations of 0.97 and 0.80 between replicates for 1 μg and 1 ng DNA samples, respectively. MID-RRBS 10, 3, 1, and 0.3 ng datasets presented average correlations of 0.95, 0.96, 0.95, 0.88 with Zymo 1 μg datasets, compared to an average correlation of 0.87 between Zymo 1 ng and 1 μg datasets. We also compared MID-RRBS data to ENCODE WGBS data (GSE 86765) of the same cell line. MID-RRBS samples of 10 and 0.3 ng recovered 9.5% and 7.7% of the CpGs detected by WGBS, respectively. Pearson coefficients between the WGBS and MID-RRBS data ranged from 0.62 to 0.70 (Supplementary Fig. 5). We also examined the breath of coverage of various genomic regions by MID-RRBS data (Fig. 2c). Although there was gradual decline in the breath of coverage for all genomic regions with decreased DNA amount, MID-RRBS samples of 1 ng or less preserved most of the coverage achieved by 10 ng samples. For example, minor decreases from 66.6% to 63.7% with ≥1× CpG measurements and 64.5% to 61.1% with ≥5× CpG measurements were observed for core promoters when the sample size changed from 10 ng to 0.3 ng. Compared to data obtained by Zymo kit, MID-RRBS data covered a particularly large percentage of

these genomic regions with ≥100× CpG measurements (Fig. 2c). For example, the percentage of core promoters covered by ≥100× CpG measurements was 53.8% at 10 ng, 48.4% at 1 ng and 47.4% at 0.3 ng using MID-RRBS, compared to 50.4% at 1 μg and 37.6% at 1 ng using the Zymo kit. We also compared MID-RRBS data with the Zymo data and other published data[30,34], in terms of the number of CpGs at various coverages (Fig. 2d) and sequencing saturation (Fig. 2e). Our data yielded very high number of CpGs with high coverage (especially >50×) compared to the Zymo data (1 μg and 1 ng), mRRBS data (100 ng using gel-free method)[30], and LCM-RRBS (1 ng)[34] (Fig. 2d). Saturation analysis revealed that our datasets taken with 1–10 ng DNA yielded higher CpG detection efficiency at all sequencing depths than competing works with the exception of the Zymo 1 μg samples (Fig. 2e). The enrichment of CpGs in various genomic contexts did not present systematic or drastic variations as the sample size changed from 10 to 0.3 ng DNA (Supplementary Fig. 6).

The MID-RRBS system facilitated highly paralleled operations. We designed a MID-RRBS system that run 4 parallel units simultaneously (Supplementary Fig. 7a and Supplementary Table 2). The inlet at the bottom allowed loading of equal amounts of various reagents into 4 units during the steps. The 4-unit system produced high-quality data (covering averagely 97.7% or 2.72 million unique CpGs with 1 ng DNA per unit) and very high reproducibility among units (with an average Pearson's correlation of 0.948, Supplementary Fig. 7b).

Although not specifically designed for single-cell operation, our device allowed studies of single cell methylomes when a group of single cell samples (24 including 2 negative controls) were indexed and processed in the single-unit device. Among the 22 single-cell RRBS datasets produced, we discarded 4 datasets with less than 35% aligned reads (sc4, sc5, sc13, and sc14 in Supplementary Table 3). The remaining 18 datasets had 35.1–72.4% (averagely 56.0%) aligned reads, in comparison to 23.9% yielded by the two negative controls, and covered 35k-231k CpGs in the genome. The number of CpGs covered had the potential to increase with high sequencing depth (Supplementary Table 3). Phi correlation coefficients among the 18 single-cell methylomes of GM12878 cells were in the range of 0.63–1.00 (Supplementary Fig. 8a). Three datasets (sc11, sc16 and sc18) appeared to be outliers of the group and the average Phi correlation among 15 datasets without the three was 0.98. The mCG/CG level in various genomic regions obtained by averaging the single cell data (18 sets) was in good agreement with that measured in 1 ng DNA MID-RRBS experiments (Supplementary Fig. 8b).

CG methylation features of NeuN+ and NeuN− fractions from mouse cerebellum are cell-type-specific

We demonstrated the utility of MID-RRBS for studying primary cell samples by examining DNA methylomes in NeuN+ and NeuN− fractions isolated from mouse cerebellum. Methylomic landscapes are important molecular features for defining cellular identities. NeuN+ and NeuN− from human and mouse frontal cortex were previously profiled by WGBS (MethylC-seq), revealing significant cell-type specific methylomic features and associated gene activities [4,5]. In contrast, previous reports on methylomes of mouse

cerebellums only included profiles on mixed nuclei population without separate methylomes on neurons and glia [35,36].

In these experiments, we isolated nuclei from mouse cerebellum samples, separated NeuN+ and NeuN− fractions by fluorescence activated cell sorting (FACS) (Fig. 3a and Supplementary Fig. 9), and used MID-RRBS to examine the methylomes. NeuN labeling has been widely used to differentiate neuronal and glial fractions[37]. However, it is worth noting that some types of cerebellar neurons including Purkinje and Golgi cells do not express NeuN[37,38]. We applied MID-RRBS to 10 and 0.5 ng DNA samples extracted from NeuN+ and NeuN− nuclei and achieved bisulfite conversion rate of 99.7 ± 0.1% (Supplementary Table 4). Our data on the cerebellum homogenate (i.e. mixed nuclei population of neurons and glia) correlated well with the RRBS data in the literature (with an average Pearson correlation of 0.90) [35]. Pearson correlation coefficients for replicates of RRBS data on individual cell types were 0.98, 0.99, 0.97, and 0.98 for 10 ng NeuN+, 10 ng NeuN-, 0.5 ng NeuN+, and 0.5 ng NeuN− samples, respectively (Supplementary Fig. 10). The numbers of CpGs discovered in these samples were slightly lower than those of GM12878 samples of similar quantities (Supplementary Table 1). Our RRBS data revealed that DNA methylation was more prevalent in NeuN− than in NeuN+ in CG context (3.9% vs 2.9% by 10 ng data and 4.1% vs 2.6% by 0.5 ng data for NeuN− and NeuN+, respectively, $p < 0.05$), but similar in CH context (0.16 % vs 0.18% by 10 ng data and 0.21% vs 0.23% by 0.5 ng data for NeuN− and NeuN+, respectively). We examined 100 most variably methylated CpG islands across NeuN+ and NeuN− methylomes using unsupervised hierarchical clustering (Fig. 3b). There were substantial methylomic differences between the two cell types. The methylomes obtained using the homogenate containing mixed neurons and glia generally reflected the average over the two cell types (Fig. 3b and Supplementary Fig. 11). We show some examples of genes having various methylation and expression levels in NeuN+, NeuN− and homogenate (Fig. 3c).

We next examined CG methylation status in several categories of annotated gene features (promoters, intergenic regions, CpG islands, and CGI shores). The methylation levels in NeuN− were significantly higher than those in NeuN+ in all categories except CpG islands (Fig. 4a). Promoters presented the most significant difference ($p < 10^{-15}$, paired t-test). The methylation profiles were highly reproducible between two replicates for all gene features (with an average Pearson correlation of 0.98). CpG islands were the most conserved feature across NeuN+ and NeuN− (Pearson coefficient up to 0.812, Fig. 4b), followed by CGI shores (up to 0.763).

We also examined how the CpG density of promoters affected their cell-type specificity. We classified the promoters into three categories: High CpG-density Promoters (HCPs, CpG Ratio > 0.6 and GC% > 0.55, n = 11410), Intermediate CpG-density Promoters (ICPs, 0.4 ≤ CpG Ratio ≤ 0.6, n = 3338), and Low CpG-density Promoters (LCPs, CpG Ratio < 0.4, n = 3014)[39]. Previous works revealed that CpGs in LCPs tend to be methylated whereas CpGs in HCPs tend to be unmethylated [39–42]. HCPs are associated with ubiquitous housekeeping and developmental genes whereas LCPs are associated with tissue-specific genes [42]. Our data strongly supported this notion. Our HCPs and ICPs were largely conserved across cell types (e.g. the average Pearson correlation coefficients were 0.83 and 0.81 between NeuN+ and

NeuN− for HCPs and ICPs, respectively) and provided only weak cell type classifications (Fig. 5). In contrast, LCPs showed strong differential CG methylation with cell-type specificity. Pearson correlations between NeuN+ and NeuN− had an average of 0.59 when LCPs were examined.

CG-differentially methylated region-associated genes have little overlap with differentially expressed genes across the two cell types from mouse cerebellum

We identified 2677 and 1649 differentially CG-methylated regions (DMRs) ($p < 0.05$), corresponding to 2184 and 1393 DMR-associated genes (Supplementary Tables 5 and 6), by comparing NeuN+ and NeuN− methylomes established using 10 ng and 0.5 ng samples, respectively (Fig. 6a). A large fraction of the two sets of genes (i.e. 60% of the DMR-associated genes detected using 0.5 ng samples) overlapped. CG-DMRs discovered using 10 ng or 0.5 ng DNA showed highly consistent distributions in various genomic features (annotated by Homer) (Supplementary Fig. 12). The DMRs were largely located around genes (averagely 71%, within ± 1 kb of RefSeq genes). We performed unbiased gene ontology (GO) analyses on DMR-associated genes and found that these genes were strongly enriched in a number of neuron or glia-specific GO terms ($p < 0.001$, hypergeometric test, Supplementary Tables 7 and 8). Some of these genes (e.g. *Neurog2, Pax5, Foxn4, Lhx6, Wnt11, Ier2, Esr2, Grik3, Cacna1b,* and *Epha2*) play important roles in neuronal and synaptic development and functions.

In order to examine the impact of methylomic features on transcription, we also performed transcriptome profiling (mRNA-seq) on NeuN+ and NeuN− subpopulations of the nuclei (Supplementary Table 9 and Supplementary Fig. 13) and identified 2331 differentially expressed genes (DE genes) between the two cell types (> 8-fold change, $p < 0.05$, t-test) (Supplementary Table 10). The mRNA-seq data on the homogenate correlated very well with the ENCODE data (with an average Pearson correlation of 0.94, GSE93456). Only 299 (14%) of CG-DMR-associated genes identified using 10 ng datasets and 182 (13%) of those identified using 0.5 ng datasets exhibited differentiated expressions in the two cell types (Fig. 6a), suggesting that there were mechanisms other than CG methylation that strongly affected transcription.

Consistent with previous report [43], CG methylation on both CGI and non-CGI promoters were associated with transcriptional repression in both cell types (Fig. 6b). In contrast, CH methylation detected by MID-RRBS did not present correlation with the level of transcription (Supplementary Fig. 14). Furthermore, the difference in CG methylation between NeuN+ and NeuN− fractions was correlated with the ratio between the expression levels across the two cell types for CGI promoters, but not for non-CGI promoters (Supplementary Fig. 15).

Detection of methylomic variations in NeuN+ fraction of mouse frontal cortex after chronic administration of an atypical antipsychotic drug

Atypical antipsychotic drugs such as clozapine are routinely used in the clinic to treat schizophrenia and other psychotic disorders [44]. Chronic administration of these drugs leads to a partial or complete remission of psychotic symptoms, including hallucinations and

delusions. Our previous work showed that chronic administration of clozapine led to changes in epigenomic features such as histone acetylation via upregulated expression of histone deacetylases (HDAC2)[45]. In here, we applied the MID-RRBS assay to study methylomic variations in NeuN+ (neuronal) fraction from frontal cortex of mice that were chronically treated with clozapine (10 mg/kg, n = 6) or vehicle (0.9% saline solution, n = 6) (Supplementary Table 11). This brain region has been involved in processes related to cognition, perception and mood. The data were highly reproducible between technical replicates (average r = 0.968, Fig. 7a). In contrast, the cross correlations among individual mice in the same group indicated substantial variation (average r = 0.836 and 0.793 for clozapine and vehicle groups, respectively). Few reports addressed the variations of epigenomic landscapes across individuals of the same species [46–48]. Our data, in agreement with the previous literature, suggested substantial variations in the NeuN+ methylome across individuals of inbred mice [47,48]. We identified 520 CG-DMRs between the treated and control groups (Fig. 7b and Supplementary Table 12), the majority of which were located around genes (79%). A number of these DMR-associated genes (listed in Supplementary Table 13) are known to be associated with schizophrenia and other mental disorders, including *Disc1* [49], *Grin2c* [50], *Npas2* [51], and *Neurod1* [52]. Interestingly, the significant changes in CG methylation level at these genes did not necessarily result in significant variation in gene expression (Supplementary Fig. 16), as indicated by mRNA-seq data (Supplementary Table 14). These results suggest that chronic administration of the atypical antipsychotic clozapine leads to significant measurable changes in the methylome of cortical neurons in genes potentially related to the therapeutic action of the drug.

Discussion

Our MID-RRBS technology offers capability for low-input profiling of DNA methylomes, taking advantage of a microfluidic system. The diffusion-based reagent exchange method permits loading/releasing of various small-molecule reagents without substantial loss in the DNA amount. Such approach facilitates conducting a complex molecular biology treatment in a microfluidic device with a simple structure. The microfluidic system and simple device design also permit processing of multiple samples simultaneously in parallel. In principle, similar approaches can be applied to WGBS. One limitation with the technology in its current form is that library preparation is conducted off the microfluidic system.

Profiling and comparing methylomes are critical for understanding difference in epigenetic regulations among various cell types in the same organ. Cell-type-specific methylome is an important part of the overall molecular machinery that defines cellular identity. In this study, we showed that our low-input MID-RRBS technology allowed us to establish distinct DNA methylomes for NeuN+ and NeuN− fractions from a mouse cerebellum or frontal cortex. The high coverage for CpGs detected by MID-RRBS ensured that various methylomic features were sufficiently revealed for comparison and differentiation of the two cell types. Complementary to previous reports on brain methylomes obtained by WGBS [4,5], our RRBS data with focus on promoters and CGIs showed substantial difference between NeuN+ and NeuN− methylomes in terms of the CG methylation levels on specific genes and across various genomic contexts. We found that LCPs bore high cell-type specificity. In spite of the inverse correlation between promoter methylation and transcription within the same cell

type, there was fairly little overlap between CG-DMR-associated genes and differentially expressed genes (< 13% of DE genes and < 14% of DMR genes) when the two cell types were compared. This strongly points to the importance of other epigenetic mechanisms such as CH methylation[4,5] on shaping brain transcriptomes.

The impact of the input amount on methylomic analysis has not been detailed previously. Our 0.5 ng and 10 ng datasets on mouse cerebellum were strongly correlated (averagely r = 0.90 for NeuN+ and 0.92 for NeuN-). However, DMR-associated genes identified using the two sets of data had noticeable difference (with only 60% of DMR-associated genes detected using 0.5 ng data overlapping with those by 10 ng data), presumably due to the combined effect of imperfect correlation and decrease in the number of CpGs covered from 10 to 0.5 ng (by 12–13% on 1× CpGs and 9–16% on 10× CpGs). This calls for caution on comparing methylomic data obtained with different input amounts.

Finally, the versatility of the MID-RRBS technology also allowed us to characterize differential methylomic profiles in response to a chronic pharmacological treatment and identify CG-DMRs relevant to the targeted disorder. The characterization of the technology herein shown open up an avenue of possibilities in the study of cell-type-specific epigenomic drug profiling. The unequivocal characterization of the neuronal epigenetic features that are unique to specific disease or treatment condition would require analysis of a group of research animals and identification of a panel of relevant DMRs. The MID-RRBS technology will be a useful and versatile tool in this endeavor.

Methods

Fabrication of the microfluidic device

The polydimethylsiloxane (PDMS)-glass device was fabricated by multilayer soft lithography [22,53]. Three photomasks (1 for the control layer and 2 for the fluidic layer) were generated with the microscale patterns designed using LayoutEditor (juspertor GmbH) and printed on high-resolution (10,000 d.p.i.) transparencies. The control layer master was fabricated by spinning SU-8 2025 (Microchem) on a 3-inch silicon wafer (P(100), 380 μm thickness, University Wafers) at 500 rpm for 10 s followed by at 3000 rpm for 45 s (yielding 24 μm in SU-8 2025 thickness). The fluidic layer master was fabricated in SU-8 2025 and AZ 9260 (Clariant) on another silicon wafer with the thickness being 60 and 13 μm, respectively. The fluidic layer master was baked at 130 °C for 30 s to round AZ 9260 features so that the resulted fluidic channels could be fully closed by microscale pneumatic valves. The control layer (~0.4 cm thick) was fabricated by pouring PDMS prepolymer (General Electric silicone RTV 615, MG chemicals) with a mass ratio of A: B =5: 1 onto the control layer master in a petri dish. The fluidic layer (~80 μm thick) was fabricated by spinning PDMS (A: B=20: 1) at 500 rpm for 10 s and then at 1500 rpm for 30 s. Both layers were baked at 75 °C for 15 min. The control layer was then peeled off from the master and access holes to the control layer channels were punched. The two PDMS layers were aligned, brought into contact, and baked for 1 h at 75 °C for thermal boning. The bonded PDMS structure was peeled off from the fluidic layer master and access holes to the fluidic layer were punched. The structure was then bonded to a cover glass (0.13–0.17 mm thick, VWR) that was pre-cleaned in 27% NH_4OH: 30% H_2O_2: H_2O=1: 1: 5 (volumetric ratio) at

80 °C for 1 h. Both PDMS surface and glass surface were oxidized in plasma (PDC-32G, Harrick Plasma) for 1 min and then immediately brought into contact. The entire structure was then baked at 75 °C for 1 h to strengthen the bonding.

Cell culture

GM12878 cells were purchased from Coriel Institute for Medical Research and cultured in RPMI 1640 medium (11875–093, Gibco) plus 15% fetal bovine serum (26140–079, Gibco) and 100 U/ml penicillin-streptomycin (15140–122, Gibco) at 37 °C in a humidified incubator with 5% CO_2. Cells were sub-cultured every 2–3 days to maintain them in exponential growth phase, by refeeding with fresh medium and maintaining at no less than 100,000 cells/ml.

Cerebellum dissection

C57BL/6 male mice were purchased from Jackson Laboratories and allowed a week of acclimation in the animal facility before sacrificing. The mice were housed at 12 h light/dark cycle at 23°C with food and water ad libitum. 8–10 week old mice were anesthetized with isoflurane (3–4%) and decapitated. Cerebellum was rapidly dissected and frozen on dry ice and stored at −80 °C until used for nuclei isolation. The Institutional Animal Care and Use Committee at Virginia Tech approved this study under animal welfare assurance #A3208-01 and protocol #16-158.

Clozapine treatment and frontal cortex dissection

Experiments were performed on adult (10–20 weeks old) 129S6/SvEv male mice (Taconic Biosciences) housed at 12 h light/dark cycle at 23°C with food and water ad libitum. Handling and chronic treatment were done as previously described [45]. Briefly, mice were injected (i.p.) daily for 21 days with 10 mg/kg of clozapine dissolved in a 0.9% saline vehicle (n = 6), or vehicle in the control group (n = 6). Mice were sacrificed without anesthesia by cervical dislocation 24 h after the last injection of clozapine, or vehicle. The bilateral frontal cortex (bregma 1.90 to 1.40 mm) was dissected and frozen at −80 °C till use. Experiments were conducted in accord with the NIH guidelines, and were approved by the Virginia Commonwealth University Animal Care and Use Committee under animal welfare assurance #A3281-01 and protocol #AD10001212. All efforts were made to minimize animal suffering and the number of animals used.

Nuclei isolation from mouse cerebellum

We used a nuclei isolation protocol that was similar to previous report [54]. A cerebellum was placed in 5 ml ice-cold nuclei extraction buffer (0.32 M sucrose, 5 mM $CaCl_2$, 3 mM $Mg(Ac)_2$, 0.1 mM EDTA, 10 mM Tris-HCl and 0.1% Triton X-100) with freshly added 50 μl protease inhibitor cocktail (P8340, Sigma-Aldrich), 5 μl of 100 mM phenylmethylsulfonyl fluoride (PMSF, Sigma-Aldrich) and 5 μl of 1 M 1,4-dithiothreitol (DTT, Sigma-Aldrich). In addition, 7.5 μl of 40 U/μl RNase inhibitor (N2611, Promega) was also added when mRNA-seq was conducted. Once thawed, the tissue was homogenized by slowly doucing for 15 times with a loose pestle (D9063, Sigma-Aldrich) and 25 times with a tight pestle (D9063, Sigma-Aldrich). The homogenate was filtered with 40 μm nylon mesh cell strainer

(22363547, Fisher Scientific) and then transferred into a 15 ml centrifugation tube. The sample was centrifuged at 1000 g for 10 min. The supernatant was removed and the cell pellet was gently resuspended in 1 ml cold nuclei extraction buffer with freshly added 10 μl protease inhibitor cocktail, 1 μl of 100 mM PMSF and 1 μl of 1 M DTT. 1.5 μl of 40 U/μl RNase inhibitor was mixed with the nuclei extraction buffer when mRNA-seq was conducted. The 1 ml sample suspension was split into two 1.5-ml micro-centrifuge tubes (500 μl in each tube). Each sample (500 μl) was gently mixed with 0.75 ml of 50% iodixanol to yield 30% iodixanol solution. 50% iodixanol was prepared by adding 0.4 ml diluent (150 mM KCl, 30 mM $MgCl_2$, and 120 mM Tris-HCl, pH 7.8) to 2 ml of 60% iodixanol (D1556, Sigma). The samples were then centrifuged at 10,000 g for 20 min before the supernatant was removed. The nuclei in each tube were incubated on ice for 10 min in 0.5 ml Dulbecco's phosphate-buffered saline (14190144, Life Technologies) containing 2.0% normal goat serum (50062Z, Life Technologies). The nuclei were resuspended and then pooled together (generating ~1 ml in total). For mRNA-seq, 3 μl of 40 U/μl RNase inhibitor was added into the nuclei suspension. The integrity and the number of nuclei were checked under the microscope. 32 μl of 2 ng/μl anti-NeuN antibody conjugated with Alexa 488 (MAB377X, EMD Millipore) was incubated with the nuclei suspension (~1 ml) for 1 h at 4 °C on an end-to-end rotator. The stained samples were sorted by FACS (BD FACSAria, BD Biosciences) with 50,000 to 100,000 unlabeled nuclei used as unstained control. We typically isolated 0.5 million NeuN+ nuclei and 0.5 million NeuN− nuclei from a mouse cerebellum. The isolated nuclei were used for RNA and DNA extraction within 1 h after FACS to maintain transcriptomic and epigenomic states.

Nuclei isolation from mouse frontal cortex

Mouse frontal cortex (see above) was homogenized in homogenization phosphate buffer (8.66 mM K_2HPO_4, 1.34 mM KH_2PO_4, 0.1 M KBr and 0.25 M Sucrose). The homogenized sample was centrifuged at 1000 g for 5 min. The cell pellet was resuspended in 0.5 ml homogenization phosphate buffer and stored at −80 °C until use. For nuclei isolation, the sample was thawed and centrifuged again at 1000 g for 5 min. The pellet was resuspended in 1 ml cold nuclei extraction buffer with freshly added 10 μl protease inhibitor cocktail, 1 μl of 100 mM PMSF and 1 μl of 1 M DTT. The sample was then processed following the cerebellum nuclei exaction procedure as mentioned above.

Genomic DNA extraction

Human genomic DNA was purified from GM 12878 cells using QIAamp DNA Blood Mini Kit (Qiagen) following the manufacturer's protocol and suspended in EB buffer (Qiagen). Mouse genomic DNA was purified using QIAamp DNA Blood Midi Kit (Qiagen) from nuclei and suspended in AE buffer (10 mM Tris-Cl, 0.5 mM EDTA, pH 9.0). The eluate was reloaded on the column membrane and spun to maximize DNA yield. Mouse DNA was concentrated by ethanol precipitation and suspended in EB buffer. The extracted DNA was used for RRBS library construction without storage.

RRBS library construction

Library construction was conducted based on the protocol published by Gu et al. [11] and modified for Illunima Hi-Seq system. 5 μl genomic DNA was digested by adding 1 μl of 20

U/μl MspI enzyme (R0106S, NEB), 2 μl NEB buffer2 and 12 μl H_2O at 37 °C for 1 h and inactivated at 80 °C for 20 min. The fragment size was examined using 2.5% agarose gel (16550100, Thermo Fisher) in 0.5× TBE buffer (15581044, Thermo Fisher). The 3′ terminal of digested DNA was end-repaired and an extra A (required by adapter ligation) was added on both strands in a single reaction. 1 μl of 5 U/μl Klenow exo- enzyme (M0212M, NEB) and 1.1 μl dNTP mixture (10 mM dATP, 1 mM dGTP and 1 mM dCTP, N0446S, NEB) were added into 20 μl digested sample. Ten-fold excess of dATP was added to increase A-tailing efficiency. The sample was incubated at 30 °C for 20 min (end-repair), 37 °C for 20 min (A-tailing) and 75 °C for 20 min (enzyme inactivation). The DNA (22.1 μl) was then purified by ethanol precipitation. DNA pellet was then resuspended in 17 μl EB buffer and transferred to a new 200 μl PCR tube. 1 μl of 2000 U/μl T4 ligase (M0202T, NEB), 2 μl of supplied 10× T4 ligase buffer, and 0.6 μl NEXTflex bisulfite-seq barcode (1.6–6 μM, NOVA-511913, Bioo Scientific) were mixed with the sample for ligation. The ligation reaction was carried out at 16 °C for 16 h and followed by 65 °C for 10 min for heat inactivation. The heating of the thermal cycler lid was turned off to protect the T4 ligase. Gel-free procedure [30,55] instead of gel cutting was used for RRBS library construction. Ligated DNA (20 μl) was purified using AMPure XP beads with bead suspension to sample volumetric ratio of 1.5: 1. The DNA was eluted from Ampure beads by 20 μl EB buffer. The eluate was concentrated by ethanol precipitation and then suspended in the EB buffer for loading into the microfluidic device.

Single-cell RRBS library construction

Single-cell RRBS library construction was conducted based on the protocol published by Guo et al. [13] with minor modifications. 96-well PCR plate was preloaded with 5 μl of lysis buffer (20 mM Tris, 2 mM EDTA, 20 mM KCl, 1 mg/ml protease and 0.3% Triton X-100) in each well. Single cells were sorted into the 96 well-plate using FACS (BD FACSAria, BD Biosciences). Cells were lysed at 50 °C for 3 h and protease was heat inactivated at 75 °C for 30 min. The lysate was digested by adding 0.9 μl of 10 U/μl MspI enzyme (ER0541, Thermofisher), 1.8 μl of 10× Tango buffer and 10.3 μl H_2O into each well and heating at 37 °C for 3 h followed by inactivating at 80 °C for 20 min. 1 μl of 5 U/μl Klenow exo- enzyme (EP0421, Thermofisher), 0.8 μl dNTP mixture (1 mM dATP, 0.1 mM dGTP and 0.1 mM dCTP, N0446S, NEB) and 0.2 μl of 10× Tango buffer were added into each well of digested sample. The samples were incubated at 37 °C for 40 min and 75 °C for 15 min. 1 μl of 30 U/μl T4 ligase (EL0013, Thermofisher), 0.5 μl of 10× Tango buffer, 0.25 μl of 100 mM ATP (R0441, Thermofisher), 1 μl of NEXTflex bisulfite-seq barcode (250 times diluted by EB buffer) and 2.25 μl H_2O were mixed with each sample for ligation. The ligation reaction was carried out at 16 °C for 30 min, 4 °C for 8 h and followed by 65 °C for 20 min for heat inactivation. 24 single-cell samples were pooled, concentrated by ethanol precipitation and suspended in EB buffer for loading into the microfluidic device for processing.

Operation of the microfluidic devices

The control layer channels were filled with DI water before experiments. The on-chip pneumatic valves were actuated at 25 psi by solenoid valves (18801003–12V, ASCO Scientific) that were connected to a compressed air outlet and operated by a LabVIEW program via a computer and a data acquisition card (PCI-6509, National Instruments).

Operation of the single-unit device (Fig. 1a and Supplementary Fig. 1)—All experimental data were obtained using the single-unit device unless otherwise noted. DNA (after adapter ligation and size selection) and reagents were delivered into the microfluidic device by a syringe pump. A syringe and a connected tubing was initially filled with water. An air plug (~ 1 cm long) was created (by aspiration) in the tubing to separate water from a liquid plug of DNA sample or other reagents (aspirated from a microcentrifuge tube after the air plug formation). Our microfluidic bisulfite conversion involved several steps: ***1).*** A conversion buffer from EZ DNA methylation-lightning kit (D5030–1, Zymo) with added 1.6% Tween 20 was loaded into the syringe pump and delivered into the two loading chambers and reaction chamber from the reagent inlet. Then the valves between the loading and reaction chambers were closed and the DNA sample (with concentrations ranging roughly from 1 to 36 ng/μl) was loaded into the reaction chamber (240 nl) from the sample inlet, replacing the conversion reagents in the reaction chamber. ***2).*** The pneumatic valves were opened for 10 min to allow diffusion-based reagent exchange. The pneumatic valves were then closed. The bisulfite mix in the loading chambers was refreshed before the pneumatic valves were opened for another 10 min. This loading process was repeated one more time to reach a total diffusion time of 30 min for bisulfite mix. ***3).*** While the pneumatic valves were closed, the bisulfite mix in the loading chambers was flushed out by water (to avoid damage to the PDMS device during heating) and the hydration line on top of the reaction chamber was pressurized (at 25 psi) to minimize water loss during heating. The microfluidic device was then placed on a flat-plate thermal cycler (TC-4000, Techne) with 1 ml paraffin oil (18512, Sigma-Aldrich) added between the device and the thermal cycler surface to improve heat transfer. The device was heated at 98°C for 5 min (heat denaturation) followed by 55 °C for 1 h (sulphonation). The whole process was conducted in dark to prevent degradation of bisulfite mix. ***4)***. Freshly-prepared 0.3 M NaOH was delivered from reagent inlet into the loading chambers. Diffusion-based loading of NaOH (and releasing of bisulfite mix) was conducted for a total of 30 min while the NaOH solution in the loading chambers was refreshed after each 10-min period. The microfluidic device was then incubated at room temperature for 20 min for desulphonation (with the pneumatic valves closed). ***5).*** Converted DNA was eluted by 100 μl Tris-EDTA buffer and then purified by ethanol precipitation with the following steps. 60 μl of 5 M ammonia acetate, 4 μl of 5 μg/μl glycogen and 480 μl of ice-cold 100% ethanol were mixed with the eluate and incubated at −80 °C for 1 h. The mixture was then spun at 16,100 g for 15 min. The supernatant was discarded without disturbing the precipitated pellet. 500 μl of 70% ethanol was added before the sample was spun again at 16,100 g for 10 min. The supernatant was removed and the pellet was air dried for 10 min. The pellet was finally resuspended in 20 μl EB buffer and stored at −80 °C until use.

Operation of the 4-unit device (Supplementary Fig. 7a)—The operation procedure was similar to that for the single-unit device with minor modifications. 4 DNA samples were loaded into reaction chambers sequentially in the order of unit 1 to 4. After bisulfite conversion, the samples were also eluted sequentially to avoid cross contamination. All other steps involved were conducted simultaneously for all 4 units.

PCR amplification and sequencing of RRBS samples

The converted DNA (20 μl) was amplified by PCR (via adding 1 μl of 2.5 U/μl PfuTurbo C_x Hotstart DNA Polymerase, 5 μl of 10× PfuTurbo C_x reaction buffer, 1.25 μl of 10 mM dNTP, 3 μl of 5 μM primers, 2.5 μl of 20× EvaGreen Dye, and 17.25 μl H_2O into the DNA sample). DNA was denatured at 95 °C for 2 min, amplified in a number of cycles (95 °C for 30 s, 65 °C for 30 s and 72 °C for 45 s) depending on the amount of starting DNA (13 cycles for 10 ng, 14 cycles for 3 ng, and 16–18 cycles for 1-0.3 ng). After PCR amplification, a double size selection using AMPure XP beads was performed following the product manual. Briefly, large DNA fragments were removed by adding 30 μl AMPure bead suspension and incubating for 5 min. The beads that had large DNA bound were discarded and the supernatant was preserved. 30 μl AMPure bead suspension were then added into the supernatant and incubated for 5 min. The supernatant was discarded and DNA bound to beads was eluted into 7 μl EB buffer. Library fragment size was determined using high sensitivity DNA analysis kit (Agilent) on a TapeStation. Each library was quantified by KAPA library quantification kit (Kapa Biosystems). Each library was pooled at 10 nM for sequencing by Illumina HiSeq 4000 with single-end 50 bp read. Typically, 30–40 million reads were generated per library.

PCR amplification and sequencing of single-cell RRBS samples

The converted DNA (20 μl) was amplified by two rounds of PCR. 0.4 μl of 2.5 U/μl PfuTurbo C_x Hotstart DNA Polymerase, 5 μl of 10× PfuTurbo C_x reaction buffer, 1 μl of 10 mM dNTP, 3 μl of 5 μM primers, 2.5 μl of 20× EvaGreen Dye, and 18.1 μl H_2O were added into each DNA sample (containing barcoded DNA from 24 cells). DNA was denatured at 95 °C for 2 min, amplified for 20 cycles (95 °C for 20 s, 65 °C for 30 s and 72 °C for 1 min for each cycle). After PCR amplification, the DNA was purified twice using AMPure XP beads with beads to sample volumetric ratio of 1:1. The DNA was eluted by 17.5 μl of H_2O. The purified DNA was amplified again by adding 25 μl Phusion High-Fidelity PCR Master Mix (F531S, Thermofisher), 5 μl of 5 μM primers and 2.5 μl of 20× EvaGreen Dye. DNA was denatured at 98 °C for 2 min, amplified for 10 cycles (98 °C for 10 s, 65 °C for 30 s and 72 °C for 1 min for each cycle). The DNA was purified again by adding 50 μl of AMPure XP beads and eluted by 15 μl of EB buffer. The DNA was quantified by KAPA library quantification kit and sequenced by Illumina HiSeq 4000 with paired-end 100 bp read.

RRBS samples processed using a Zymo kit

The library preparation procedure was the same as that of RRBS library construction. Adapter-ligated DNA was bisulfite-converted using EZ DNA Methylation-Lightning Kit (D5030, Zymo) following instruction manual. The process involved a column-based DNA purification step. After conversion, the DNA was eluted to 20 μl of EB buffer.

RRBS data analysis

Sequencing reads were trimmed by trim galore with --RRBS option. The trimmed reads were aligned to hg19 or mm9 genome by bismark [56] and bowtie [57] with default settings. The bisulfite conversion rate and CpG coverage were calculated by methylKit [58] using aligned reads. The called CpGs were visualized in IGV genome browser [59]. Regional analysis was

performed for mouse data using (http://www.bioinformatics.bbsrc.ac.uk/projects/seqmonk/). Features containing at least 10 CpGs with each CpG having 25× coverage are included in the calculations. The promoters were defined as 2 kb upstream and 500 bp downstream of transcription starting sites of RefSeq genes. Intergenic regions were defined by regions other than gene bodies and promoters. CpG islands were downloaded from UCSC database. CpG shores were defined as 2 kb regions flanking CpG Islands. The promoters were classified into HCPs, ICPs, and LCPs based on CpG ratio and GC% content. The coordinates of classified promoters were obtained from literature [40]. DMRs were identified by DSS [60] ($p < 0.05$) and annotated to the closest RefSeq genes (i.e. DMR-associated genes). Genes that were closest to DMRs were extracted as targets for gene ontology (GO) term enrichment analysis by DAVID [61] ($p < 0.05$).

mRNA-seq

RNA was extracted from ~100,000 nuclei using RNeasy Mini Kit (Qiagen). DNase treatment was included following manufacturer instructions to remove gDNA contamination. The RNA quality was detected by High Sensitivity RNA ScreenTape System (Agilent) to yield RNA integrity number (RIN) > 6. mRNA-seq libraries were prepared using SMART-seq v4 Ultra Low Input RNA kit (Clontech) and Nextera XT DNA library prep kit (Illumina) following instructions. Briefly, 1 ng RNA (9.5 μl) was mixed with 1 μl of 10× reaction buffer. The sample was mixed with 2 μl of 3′ SMART-seq CDS primer II A and incubated at 72 °C for 3 min. The sample was then placed on ice for 2 min. 5.5 μl Master Mix and 2 μl SMARTScribe Reverse Transcriptase were added into the sample (20 μl in total). The mixture was incubated at 42 °C for 90 min and then 70 °C for 10 min to synthesize first-strand cDNA. cDNA was then amplified by 13 cycles of PCR. The PCR product was purified by AMPure beads. 100–150 pg purified cDNA was used for Nextera library preparation. The cDNA was tagmented at 55 °C for 5 min and neutralized at room temperature for 5 min. The tagmented DNA was amplified by 12 cycles of PCR and purified by 30 μl AMPure XP beads. The fragment size was determined by a Tapestation and quantified by KAPA qPCR library quantification kit. Each library was pooled at 10 nM for sequencing by Illumina HiSeq 4000 with single-end 50 nt read. Typically, 20 million reads were generated per library.

mRNA-seq data analysis

Sequencing reads were trimmed by trim galore with default settings. The trimmed reads were aligned by Tophat [62]. The aligned reads were further analyzed by cufflinks [63]. The gene expression level was plotted by cummerbund (http://compbio.mit.edu/cummeRbund/), Seqmonk and custom R scripts. Differentially expressed genes were identified by cummerbund.

Mathematical modelling of microfluidic diffusion

The time-lapse diffusion process in the microfluidic device was modelled using COMSOL Multiphysics 4.3 as previously described [29]. We used 1.3×10^{-9}, 9×10^{-10} and 2×10^{-11} m^2s^{-1} for diffusivities of ions, quinol and 250 bp DNA, respectively [64–66].

Data availability

The authors declare that all data supporting the findings of this study are available within the paper and its Supplementary Information. Gene Expression Omnibus: MID-RRBS and mRNA-seq data are deposited under accession number GSE88716 (https://www.ncbi.nlm.nih.gov/geo/query/acc.cgi?acc=GSE88716).

Code availability

Custom scripts and functions are available from the authors upon request.

Supplementary Material

Refer to Web version on PubMed Central for supplementary material.

Acknowledgments

We thank C. Luo, J. Lucero, M.M. Behrens, and J.R. Ecker at Salk Institute; J. Ma at Carnegie Mellon University for helpful discussion. This work was supported by US National Institutes of Health grants EB017235 (C.L.), HG009256 (C.L.), MH084894 (J.G.-M), MH111940 (J.G.-M), and NS094574 (H.X.).

References

1. Hansen KD, Timp W, Bravo HC, Sabunciyan S, Langmead B, McDonald OG, Wen B, Wu H, Liu Y, Diep D, Briem E, Zhang K, Irizarry RA, Feinberg AP. Increased methylation variation in epigenetic domains across cancer types. Nat Genet. 2011; 43:768–775. [PubMed: 21706001]
2. Spiers H, Hannon E, Schalkwyk LC, Smith R, Wong CC, O'Donovan MC, Bray NJ, Mill J. Methylomic trajectories across human fetal brain development. Genome Res. 2015; 25:338–352. [PubMed: 25650246]
3. Numata S, Ye T, Hyde TM, Guitart-Navarro X, Tao R, Wininger M, Colantuoni C, Weinberger DR, Kleinman JE, Lipska BK. DNA methylation signatures in development and aging of the human prefrontal cortex. Am J Hum Genet. 2012; 90:260–272. [PubMed: 22305529]
4. Lister R, Mukamel EA, Nery JR, Urich M, Puddifoot CA, Johnson ND, Lucero J, Huang Y, Dwork AJ, Schultz MD, Yu M, Tonti-Filippini J, Heyn H, Hu S, Wu JC, Rao A, Esteller M, He C, Haghighi FG, Sejnowski TJ, Behrens MM, Ecker JR. Global epigenomic reconfiguration during mammalian brain development. Science. 2013; 341:1237905. [PubMed: 23828890]
5. Mo A, Mukamel EA, Davis FP, Luo C, Henry GL, Picard S, Urich MA, Nery JR, Sejnowski TJ, Lister R, Eddy SR, Ecker JR, Nathans J. Epigenomic Signatures of Neuronal Diversity in the Mammalian Brain. Neuron. 2015; 86:1369–1384. [PubMed: 26087164]
6. Lister R, O'Malley RC, Tonti-Filippini J, Gregory BD, Berry CC, Millar AH, Ecker JR. Highly integrated single-base resolution maps of the epigenome in Arabidopsis. Cell. 2008; 133:523–536. [PubMed: 18423832]
7. Cokus SJ, Feng S, Zhang X, Chen Z, Merriman B, Haudenschild CD, Pradhan S, Nelson SF, Pellegrini M, Jacobsen SE. Shotgun bisulphite sequencing of the Arabidopsis genome reveals DNA methylation patterning. Nature. 2008; 452:215–219. [PubMed: 18278030]
8. Down TA, Rakyan VK, Turner DJ, Flicek P, Li H, Kulesha E, Graf S, Johnson N, Herrero J, Tomazou EM, Thorne NP, Backdahl L, Herberth M, Howe KL, Jackson DK, Miretti MM, Marioni JC, Birney E, Hubbard TJP, Durbin R, Tavare S, Beck S. A Bayesian deconvolution strategy for immunoprecipitation-based DNA methylome analysis. Nat Biotechnol. 2008; 26:779–785. [PubMed: 18612301]
9. Serre D, Lee BH, Ting AH. MBD-isolated Genome Sequencing provides a high-throughput and comprehensive survey of DNA methylation in the human genome. Nucleic Acids Res. 2010; 38:391–399. [PubMed: 19906696]

10. Meissner A, Gnirke A, Bell GW, Ramsahoye B, Lander ES, Jaenisch R. Reduced representation bisulfite sequencing for comparative high-resolution DNA methylation analysis. Nucleic Acids Res. 2005; 33:5868–5877. [PubMed: 16224102]
11. Gu H, Bock C, Mikkelsen TS, Jager N, Smith ZD, Tomazou E, Gnirke A, Lander ES, Meissner A. Genome-scale DNA methylation mapping of clinical samples at single-nucleotide resolution. Nat Methods. 2010; 7:133–136. [PubMed: 20062050]
12. Adey A, Shendure J. Ultra-low-input, tagmentation-based whole-genome bisulfite sequencing. Genome Res. 2012; 22:1139–1143. [PubMed: 22466172]
13. Guo H, Zhu P, Wu X, Li X, Wen L, Tang F. Single-cell methylome landscapes of mouse embryonic stem cells and early embryos analyzed using reduced representation bisulfite sequencing. Genome Res. 2013; 23:2126–2135. [PubMed: 24179143]
14. Smallwood SA, Lee HJ, Angermueller C, Krueger F, Saadeh H, Peat J, Andrews SR, Stegle O, Reik W, Kelsey G. Single-cell genome-wide bisulfite sequencing for assessing epigenetic heterogeneity. Nat Methods. 2014; 11:817–820. [PubMed: 25042786]
15. Farlik M, Sheffield Nathan C, Nuzzo A, Datlinger P, Schönegger A, Klughammer J, Bock C. Single-Cell DNA Methylome Sequencing and Bioinformatic Inference of Epigenomic Cell-State Dynamics. Cell Rep. 2015; 10:1386–1397. [PubMed: 25732828]
16. Luo C, Keown CL, Kurihara L, Zhou J, He Y, Li J, Castanon R, Lucero J, Nery JR, Sandoval JP, Bui B, Sejnowski TJ, Harkins TT, Mukamel EA, Behrens MM, Ecker JR. Single-cell methylomes identify neuronal subtypes and regulatory elements in mammalian cortex. Science. 2017; 357:600–604. [PubMed: 28798132]
17. Treutlein B, Brownfield DG, Wu AR, Neff NF, Mantalas GL, Espinoza FH, Desai TJ, Krasnow MA, Quake SR. Reconstructing lineage hierarchies of the distal lung epithelium using single-cell RNA-seq. Nature. 2014; 509:371–375. [PubMed: 24739965]
18. Lohr JG, Adalsteinsson VA, Cibulskis K, Choudhury AD, Rosenberg M, Cruz-Gordillo P, Francis JM, Zhang CZ, Shalek AK, Satija R, Trombetta JJ, Lu D, Tallapragada N, Tahirova N, Kim S, Blumenstiel B, Sougnez C, Lowe A, Wong B, Auclair D, Van Allen EM, Nakabayashi M, Lis RT, Lee GSM, Li T, Chabot MS, Ly A, Taplin ME, Clancy TE, Loda M, Regev A, Meyerson M, Hahn WC, Kantoff PW, Golub TR, Getz G, Boehm JS, Love JC. Whole-exome sequencing of circulating tumor cells provides a window into metastatic prostate cancer. Nat Biotechnol. 2014; 32:479–484. [PubMed: 24752078]
19. Han L, Zi X, Garmire LX, Wu Y, Weissman SM, Pan X, Fan R. Co-detection and sequencing of genes and transcripts from the same single cells facilitated by a microfluidics platform. Sci Rep. 2014; 4:6485. [PubMed: 25255798]
20. Macosko, Evan Z., Basu, A., Satija, R., Nemesh, J., Shekhar, K., Goldman, M., Tirosh, I., Bialas, Allison R., Kamitaki, N., Martersteck, Emily M., Trombetta, John J., Weitz, David A., Sanes, Joshua R., Shalek, Alex K., Regev, A., McCarroll, Steven A. Highly Parallel Genome-wide Expression Profiling of Individual Cells Using Nanoliter Droplets. Cell. 2015; 161:1202–1214. [PubMed: 26000488]
21. Gierahn TM, Wadsworth MH II, Hughes TK, Bryson BD, Butler A, Satija R, Fortune S, Love JC, Shalek AK. Seq-Well: portable, low-cost RNA sequencing of single cells at high throughput. Nat Methods. 2017; 14:395–398. [PubMed: 28192419]
22. Cao Z, Chen C, He B, Tan K, Lu C. A microfluidic device for epigenomic profiling using 100 cells. Nat Methods. 2015; 12:959–962. [PubMed: 26214128]
23. Rotem A, Ram O, Shoresh N, Sperling RA, Goren A, Weitz DA, Bernstein BE. Single-cell ChIP-seq reveals cell subpopulations defined by chromatin state. Nat Biotechnol. 2015; 33:1165–1172. [PubMed: 26458175]
24. Yoon J, Park MK, Lee TY, Yoon YJ, Shin Y. LoMA-B: a simple and versatile lab-on-a-chip system based on single-channel bisulfite conversion for DNA methylation analysis. Lab Chip. 2015; 15:3530–3539. [PubMed: 26194344]
25. Stark A, Shin DJ, Pisanic T 2nd, Hsieh K, Wang TH. A parallelized microfluidic DNA bisulfite conversion module for streamlined methylation analysis. Biomed Microdevices. 2016; 18:5. [PubMed: 26759004]

26. Ehrich M, Zoll S, Sur S, van den Boom D. A new method for accurate assessment of DNA quality after bisulfite treatment. Nucleic Acids Res. 2007; 35:e29. [PubMed: 17259213]
27. Grunau C, Clark SJ, Rosenthal A. Bisulfite genomic sequencing: systematic investigation of critical experimental parameters. Nucleic Acids Res. 2001; 29:e65. [PubMed: 11433041]
28. Munson K, Clark J, Lamparska-Kupsik K, Smith SS. Recovery of bisulfite-converted genomic sequences in the methylation-sensitive QPCR. Nucleic Acids Res. 2007; 35:2893–2903. [PubMed: 17439964]
29. Ma S, Loufakis DN, Cao Z, Chang Y, Achenie LEK, Lu C. Diffusion-based microfluidic PCR for “one-pot” analysis of cells. Lab Chip. 2014; 14:2905–2909. [PubMed: 24921711]
30. Boyle P, Clement K, Gu H, Smith ZD, Ziller M, Fostel JL, Holmes L, Meldrim J, Kelley F, Gnirke A, Meissner A. Gel-free multiplexed reduced representation bisulfite sequencing for large-scale DNA methylation profiling. Genome Biol. 2012; 13:R92. [PubMed: 23034176]
31. Guo S, Diep D, Plongthongkum N, Fung HL, Zhang K, Zhang K. Identification of methylation haplotype blocks aids in deconvolution of heterogeneous tissue samples and tumor tissue-of-origin mapping from plasma DNA. Nat Genet. 2017; 49:635–642. [PubMed: 28263317]
32. Zhou J, Yang L, Zhong T, Mueller M, Men Y, Zhang N, Xie J, Giang K, Chung H, Sun X, Lu L, Carmichael GG, Taylor HS, Huang Y. H19 lncRNA alters DNA methylation genome wide by regulating S-adenosylhomocysteine hydrolase. Nature communications. 2015; 6:10221.
33. Xu RH, Wei W, Krawczyk M, Wang W, Luo H, Flagg K, Yi S, Shi W, Quan Q, Li K, Zheng L, Zhang H, Caughey BA, Zhao Q, Hou J, Zhang R, Xu Y, Cai H, Li G, Hou R, Zhong Z, Lin D, Fu X, Zhu J, Duan Y, Yu M, Ying B, Zhang W, Wang J, Zhang E, Zhang C, Li O, Guo R, Carter H, Zhu JK, Hao X, Zhang K. Circulating tumour DNA methylation markers for diagnosis and prognosis of hepatocellular carcinoma. Nature materials. 2017; 16:1155–1161. [PubMed: 29035356]
34. Schillebeeckx M, Schrade A, Lobs AK, Pihlajoki M, Wilson DB, Mitra RD. Laser capture microdissection-reduced representation bisulfite sequencing (LCM-RRBS) maps changes in DNA methylation associated with gonadectomy-induced adrenocortical neoplasia in the mouse. Nucleic Acids Res. 2013; 41:e116. [PubMed: 23589626]
35. Reizel Y, Spiro A, Sabag O, Skversky Y, Hecht M, Keshet I, Berman BP, Cedar H. Gender-specific postnatal demethylation and establishment of epigenetic memory. Genes Dev. 2015; 29:923–933. [PubMed: 25934504]
36. Gabel HW, Kinde BZ, Stroud H, Gilbert CS, Harmin DA, Kastan NR, Hemberg M, Ebert DH, Greenberg ME. Disruption of DNA methylation-dependent long gene repression in Rett syndrome. Nature. 2015; 522:89–93. [PubMed: 25762136]
37. Mullen RJ, Buck CR, Smith AM. NeuN, a neuronal specific nuclear protein in vertebrates. Development. 1992; 116:201–211. [PubMed: 1483388]
38. Weyer A, Schilling K. Developmental and cell type-specific expression of the neuronal marker NeuN in the murine cerebellum. J Neurosci Res. 2003; 73:400–409. [PubMed: 12868073]
39. Weber M, Hellmann I, Stadler MB, Ramos L, Paabo S, Rebhan M, Schubeler D. Distribution, silencing potential and evolutionary impact of promoter DNA methylation in the human genome. Nat Genet. 2007; 39:457–466. [PubMed: 17334365]
40. Mikkelsen TS, Ku M, Jaffe DB, Issac B, Lieberman E, Giannoukos G, Alvarez P, Brockman W, Kim TK, Koche RP, Lee W, Mendenhall E, O’Donovan A, Presser A, Russ C, Xie X, Meissner A, Wernig M, Jaenisch R, Nusbaum C, Lander ES, Bernstein BE. Genome-wide maps of chromatin state in pluripotent and lineage-committed cells. Nature. 2007; 448:553–560. [PubMed: 17603471]
41. Davies MN, Volta M, Pidsley R, Lunnon K, Dixit A, Lovestone S, Coarfa C, Harris RA, Milosavljevic A, Troakes C, Al-Sarraj S, Dobson R, Schalkwyk LC, Mill J. Functional annotation of the human brain methylome identifies tissue-specific epigenetic variation across brain and blood. Genome Biol. 2012; 13:R43. [PubMed: 22703893]
42. Meissner A, Mikkelsen TS, Gu H, Wernig M, Hanna J, Sivachenko A, Zhang X, Bernstein BE, Nusbaum C, Jaffe DB, Gnirke A, Jaenisch R, Lander ES. Genome-scale DNA methylation maps of pluripotent and differentiated cells. Nature. 2008; 454:766–770. [PubMed: 18600261]
43. Angermueller C, Clark SJ, Lee HJ, Macaulay IC, Teng MJ, Hu TX, Krueger F, Smallwood SA, Ponting CP, Voet T, Kelsey G, Stegle O, Reik W. Parallel single-cell sequencing links

transcriptional and epigenetic heterogeneity. Nat Methods. 2016; 13:229–232. [PubMed: 26752769]

44. Meltzer HY. Update on typical and atypical antipsychotic drugs. Annual review of medicine. 2013; 64:393–406.
45. Kurita M, Holloway T, Garcia-Bea A, Kozlenkov A, Friedman AK, Moreno JL, Heshmati M, Golden SA, Kennedy PJ, Takahashi N, Dietz DM, Mocci G, Gabilondo AM, Hanks J, Umali A, Callado LF, Gallitano AL, Neve RL, Shen L, Buxbaum JD, Han MH, Nestler EJ, Meana JJ, Russo SJ, Gonzalez-Maeso J. HDAC2 regulates atypical antipsychotic responses through the modulation of mGlu2 promoter activity. Nat Neurosci. 2012; 15:1245–U1109. [PubMed: 22864611]
46. Kasowski M, Kyriazopoulou-Panagiotopoulou S, Grubert F, Zaugg JB, Kundaje A, Liu Y, Boyle AP, Zhang QC, Zakharia F, Spacek DV, Li J, Xie D, Olarerin-George A, Steinmetz LM, Hogenesch JB, Kellis M, Batzoglou S, Snyder M. Extensive variation in chromatin states across humans. Science. 2013; 342:750–752. [PubMed: 24136358]
47. Feinberg AP, Irizarry RA. Stochastic epigenetic variation as a driving force of development, evolutionary adaptation, and disease. Proc Natl Acad Sci USA. 2010; 107:1757–1764. [PubMed: 20080672]
48. Oey H, Isbel L, Hickey P, Ebaid B, Whitelaw E. Genetic and epigenetic variation among inbred mouse littermates: identification of inter-individual differentially methylated regions. Epigenetics Chromatin. 2015; 8:54. [PubMed: 26692901]
49. Millar JK, Wilson-Annan JC, Anderson S, Christie S, Taylor MS, Semple CA, Devon RS, St Clair DM, Muir WJ, Blackwood DH, Porteous DJ. Disruption of two novel genes by a translocation co-segregating with schizophrenia. Hum Mol Genet. 2000; 9:1415–1423. [PubMed: 10814723]
50. Ayalew M, Le-Niculescu H, Levey DF, Jain N, Changala B, Patel SD, Winiger E, Breier A, Shekhar A, Amdur R, Koller D, Nurnberger JI, Corvin A, Geyer M, Tsuang MT, Salomon D, Schork NJ, Fanous AH, O'Donovan MC, Niculescu AB. Convergent functional genomics of schizophrenia: from comprehensive understanding to genetic risk prediction. Mol Psychiatry. 2012; 17:887–905. [PubMed: 22584867]
51. Cukier HN, Dueker ND, Slifer SH, Lee JM, Whitehead PL, Lalanne E, Leyva N, Konidari I, Gentry RC, Hulme WF, Booven DV, Mayo V, Hofmann NK, Schmidt MA, Martin ER, Haines JL, Cuccaro ML, Gilbert JR, Pericak-Vance MA. Exome sequencing of extended families with autism reveals genes shared across neurodevelopmental and neuropsychiatric disorders. Mol Autism. 2014; 5:1. [PubMed: 24410847]
52. Lee BJ, Marchionni L, Andrews CE, Norris AL, Nucifora LG, Wu YC, Wright RA, Pevsner J, Ross CA, Margolis RL, Sawa A, Nucifora FC Jr. Analysis of differential gene expression mediated by clozapine in human postmortem brains. Schizophrenia research. 2017; 185:58–66. [PubMed: 28038920]
53. Unger MA, Chou HP, Thorsen T, Scherer A, Quake SR. Monolithic microfabricated valves and pumps by multilayer soft lithography. Science. 2000; 288:113–116. [PubMed: 10753110]
54. Lake BB, Ai R, Kaeser GE, Salathia NS, Yung YC, Liu R, Wildberg A, Gao D, Fung HL, Chen S, Vijayaraghavan R, Wong J, Chen A, Sheng X, Kaper F, Shen R, Ronaghi M, Fan JB, Wang W, Chun J, Zhang K. Neuronal subtypes and diversity revealed by single-nucleus RNA sequencing of the human brain. Science. 2016; 352:1586–1590. [PubMed: 27339989]
55. Lister R, Pelizzola M, Kida YS, Hawkins RD, Nery JR, Hon G, Antosiewicz-Bourget J, O/'Malley R, Castanon R, Klugman S, Downes M, Yu R, Stewart R, Ren B, Thomson JA, Evans RM, Ecker JR. Hotspots of aberrant epigenomic reprogramming in human induced pluripotent stem cells. Nature. 2011; 471:68–73. [PubMed: 21289626]
56. Krueger F, Andrews SR. Bismark: a flexible aligner and methylation caller for Bisulfite-Seq applications. Bioinformatics. 2011; 27:1571–1572. [PubMed: 21493656]
57. Langmead B, Trapnell C, Pop M, Salzberg SL. Ultrafast and memory-efficient alignment of short DNA sequences to the human genome. Genome Biol. 2009; 10:R25. [PubMed: 19261174]
58. Akalin A, Kormaksson M, Li S, Garrett-Bakelman FE, Figueroa ME, Melnick A, Mason CE. methylKit: a comprehensive R package for the analysis of genome-wide DNA methylation profiles. Genome Biol. 2012; 13:2012–2013.

59. Robinson JT, Thorvaldsdottir H, Winckler W, Guttman M, Lander ES, Getz G, Mesirov JP. Integrative genomics viewer. Nat Biotechnol. 2011; 29:24–26. [PubMed: 21221095]
60. Wu H, Wang C, Wu Z. A new shrinkage estimator for dispersion improves differential expression detection in RNA-seq data. Biostatistics (Oxford, England). 2013; 14:232–243.
61. Dennis G, Sherman BT, Hosack DA, Yang J, Gao W, Lane HC, Lempicki RA. DAVID: Database for Annotation, Visualization, and Integrated Discovery. Genome Biol. 2003; 4:R60.
62. Trapnell C, Pachter L, Salzberg SL. TopHat: discovering splice junctions with RNA-Seq. Bioinformatics. 2009; 25:1105–1111. [PubMed: 19289445]
63. Trapnell C, Williams BA, Pertea G, Mortazavi A, Kwan G, van Baren MJ, Salzberg SL, Wold BJ, Pachter L. Transcript assembly and quantification by RNA-Seq reveals unannotated transcripts and isoform switching during cell differentiation. Nat Biotechnol. 2010; 28:511–515. [PubMed: 20436464]
64. Samson E, Marchand J, Snyder KA. Calculation of ionic diffusion coefficients on the basis of migration test results. Mater Struct. 2003; 36:156–165.
65. Hayduk W, Laudie H. Prediction of diffusion coefficients for nonelectrolytes in dilute aqueous solutions. AIChE J. 1974; 20:611–615.
66. Nkodo AE, Garnier JM, Tinland B, Ren H, Desruisseaux C, McCormick LC, Drouin G, Slater GW. Diffusion coefficient of DNA molecules during free solution electrophoresis. Electrophoresis. 2001; 22:2424–2432. [PubMed: 11519946]

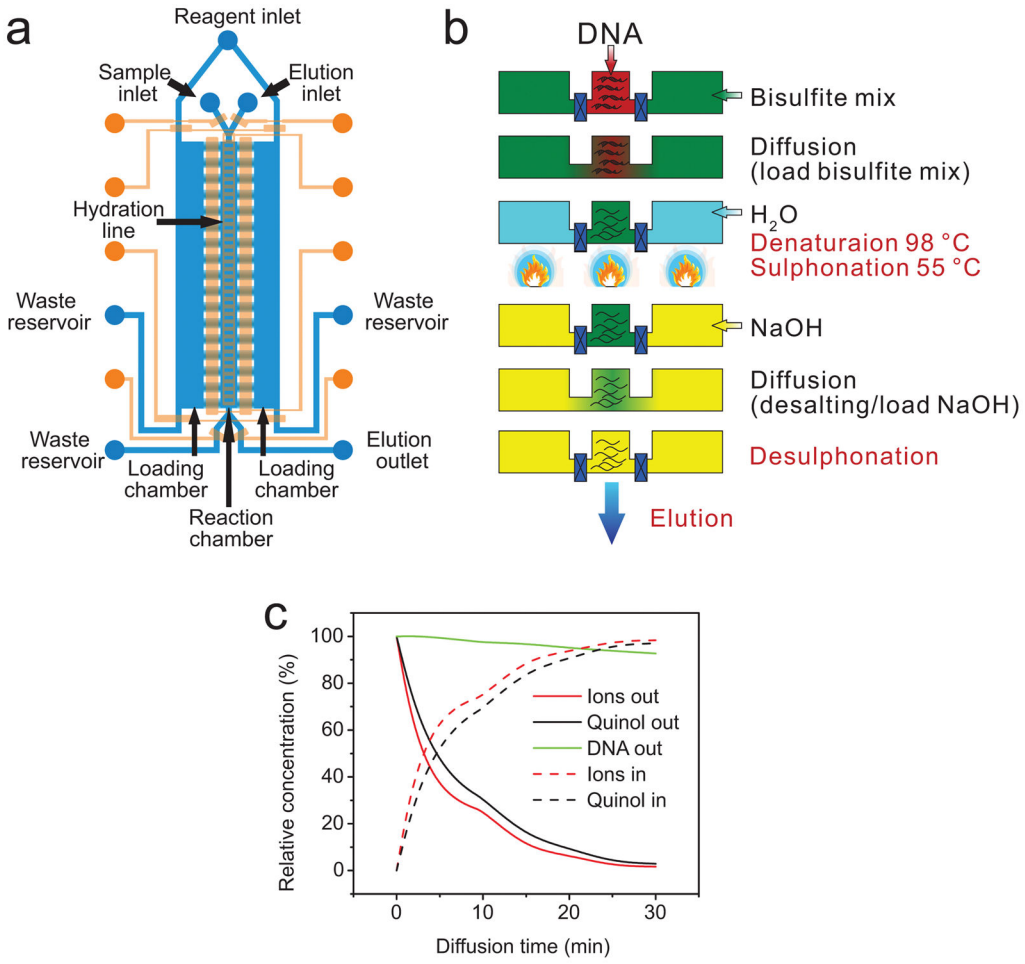

Figure 1. MID-RRBS device and protocol

(a) A schematic illustration of the two-layered microfluidic device with the fluidic layer labeled blue and the control layer labeled orange. The device (a single-unit device) consisted of one reaction chamber at the center and two connected loading chambers. A hydration line containing water within the control layer was pressurized during heating to minimize water loss from the reaction chamber. (b) Steps involved in MID-RRBS. The schematics were drawn with a cross-sectional view of the three chambers. (c) COMSOL modelling of release (solid lines) and loading (broken lines) of various molecular species from/into the reaction chamber. The release and loading of the molecules were conducted in three diffusion periods of 10 min each with the solution in the loading chambers refreshed after each period. The initial concentration in the loading chambers was considered as 100% in the case of loading whereas the one in the reaction chamber as 100% for release.

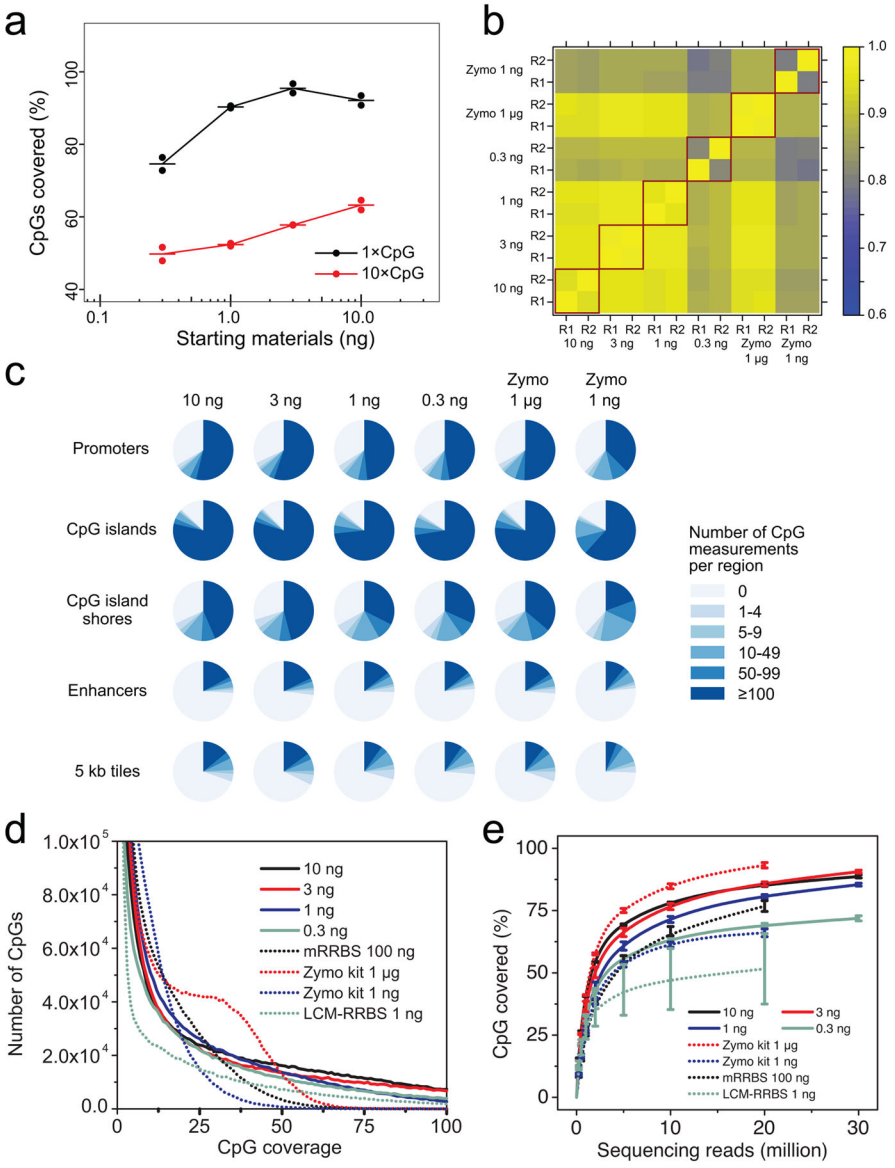

Figure 2. MID-RRBS generated high quality data using sub-1 ng DNA

(a) The percentage of the theoretical maximum of CpGs covered at 1× and 10× coverage with starting DNA samples of various amounts. MspI *in silico* digestion followed by size selection of the hg19 genome produces the theoretical maximum of 2,782,793 CpGs. The centre represents mean. (b) Pearson's correlations in the CG methylation level among various samples processed by MID-RRBS and Zymo kit. CpGs with ≥25× coverage were examined in the calculations. n = 14871. (c) MID-RRBS coverage of gene promoters (2 kb regions upstream of transcription starting sites of RefSeq genes), CpG islands (UCSC annotation database), CpG island shores (2 kb regions adjacent to CpG islands), enhancers (regions defined by H3K4me1+ H3K27ac based on ENCODE ChIP-seq data of GM12878 cells, ENCFF001SUE and ENCFF660QDF), and 5 kb tiles (non-overlapping consecutive 5 kb windows), in comparison to those of 1 μg and 1 ng samples processed by the Zymo kit. (d) The number of CpGs with various coverages (0–100×), in comparison to those of data

produced using Zymo kit, mRRBS[30], and LCM-RRBS [34]. (e) Saturation analysis of MID-RRBS data in comparison with other works. The analysis was conducted by random selection of a number of raw reads followed by using the same pipeline to identify unique CpGs. Each data point was generated with 4 subsamplings per dataset. The error bars represent s.d. The centre represents mean. n = 3 for LCM-RRBS, n = 8 for mRRBS, n = 2 for the rest.

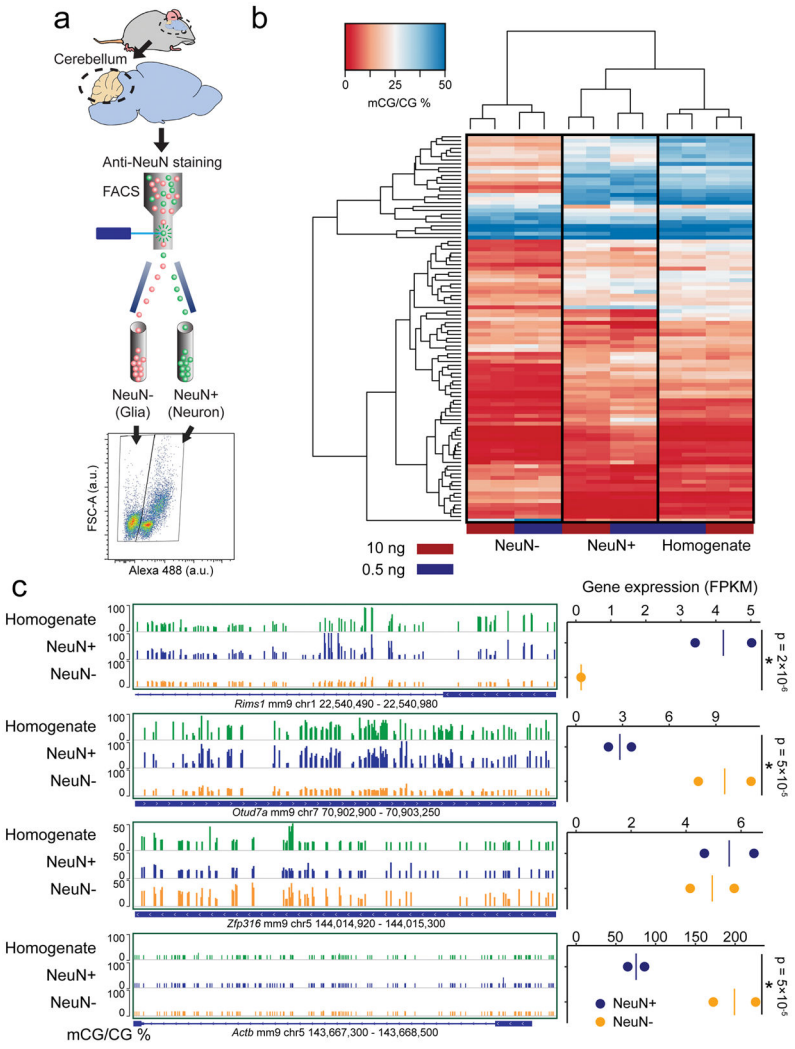

Figure 3. Distinct methylomic features in NeuN+ and NeuN− fractions from mouse cerebellum

(a) Separation of NeuN+ and NeuN− fractions from mouse cerebellum using FACS. (b) Heat map depicting unsupervised clustering analysis of 100 most variably methylated CpG islands (CG methylation) between NeuN+ and NeuN−. CpG islands containing more than 10 CpGs with each CpG having ≥ 25× coverage are included in the heat map. (c) CG methylation at various genes in NeuN+, NeuN− and homogenate (10 ng DNA per sample). Their associated expression levels are also shown. * represents p value < 10^{-4} (two-sided t-test, n = 2). The centre represents mean.

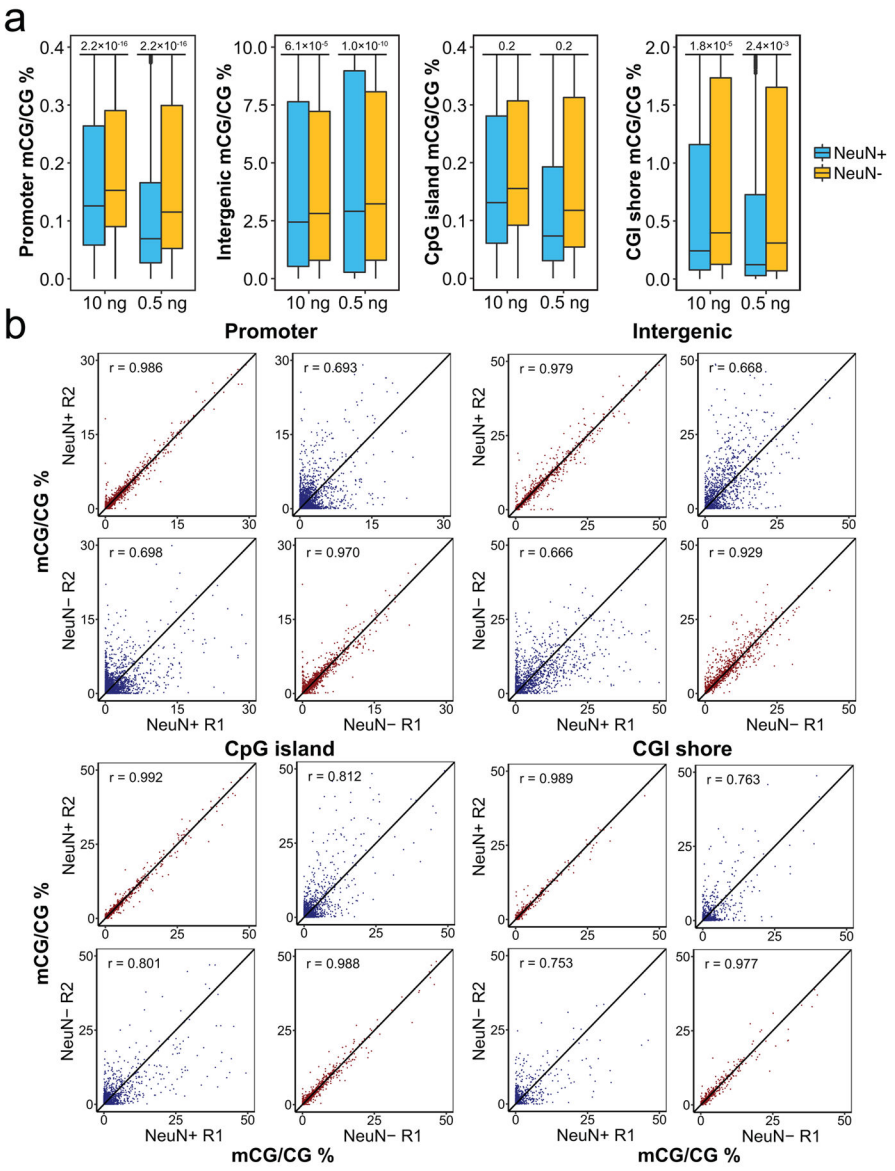

Figure 4. CG methylation levels across various annotated genomic features for NeuN+ and NeuN − fractions from mouse cerebellum

(a) Box plots of CG methylation levels in promoters (n = 23525), intergenic regions (n = 19239), CpG islands (n = 16027), and CpG island shores (n = 30232). The boxes represent first quartile, median, and third quartile. Dots represent outliers. P-values are calculated using paired two-sided t-test and shown on top of the plots. (b) Scatter plots of CG methylation levels in promoters, intergenic regions, CpG islands, and CpG island shores. The MID-RRBS data were generated using 0.5 ng NeuN+/NeuN− DNA. r represents Pearson coefficient. R1 and R2 are two replicates.

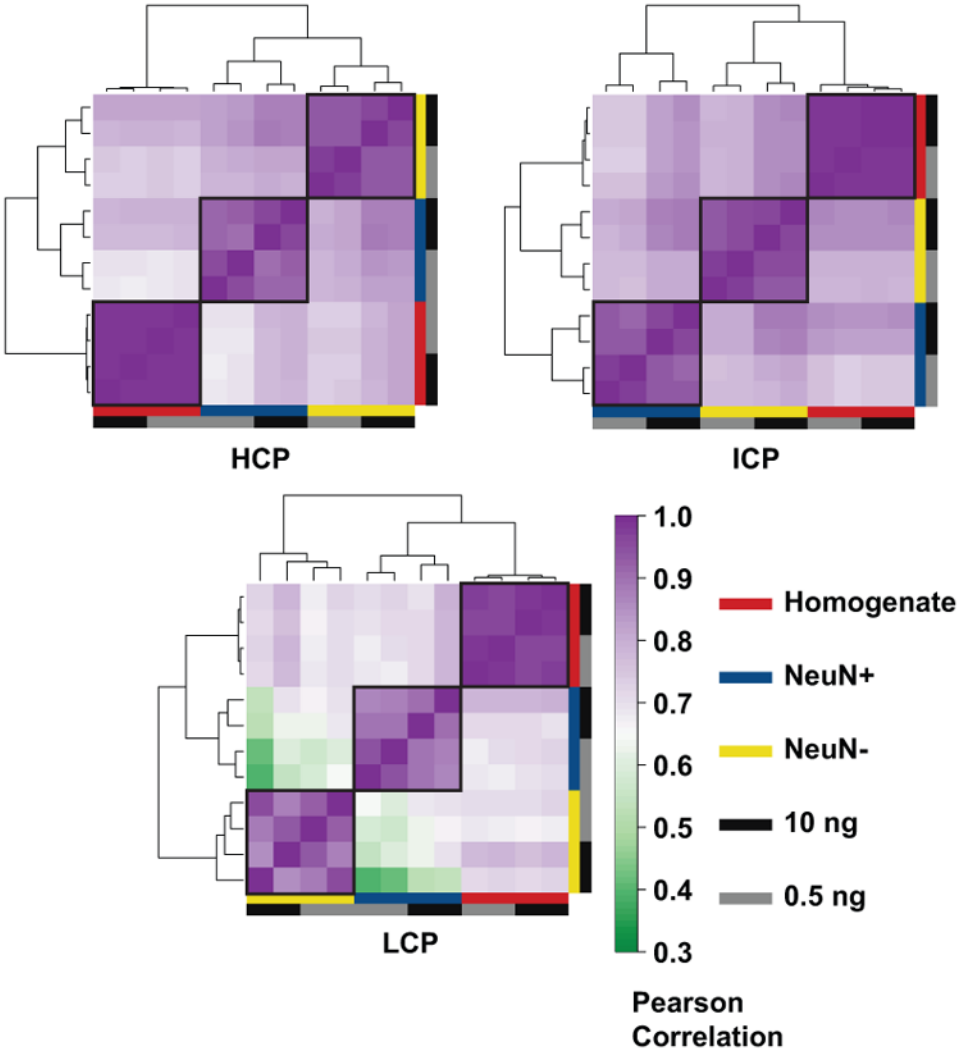

Figure 5. Pearson's correlations in CG methylation levels for low, intermediate, and high CpG density promoters (LCP, ICP, and HCP) among homogenate, NeuN+, and NeuN− samples

Promoters containing more than 5 CpGs with each CpG having ≥ 5× coverage are included in the calculations. n = 3014, 3338, and 11410 for LCP, ICP, and HCP, respectively.

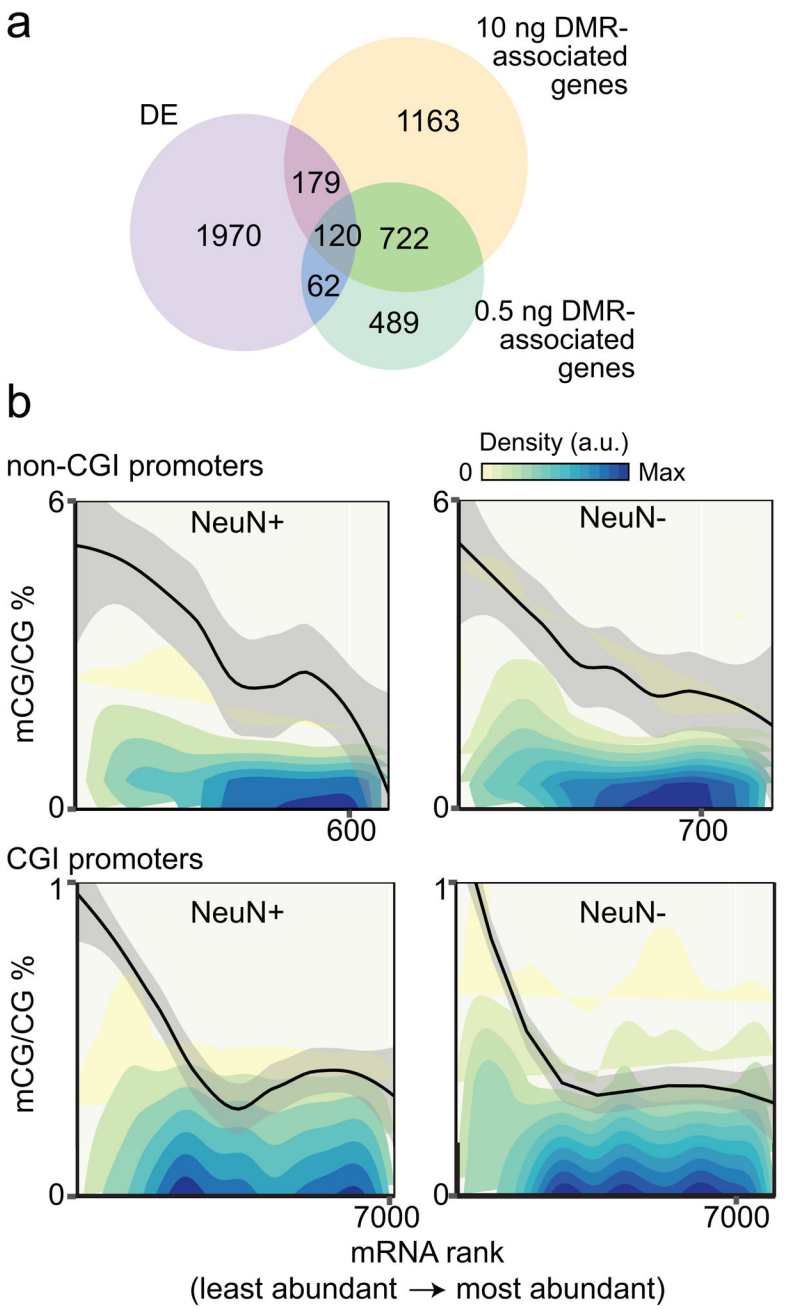

Figure 6. Interactions between methylomes and transcriptomes for NeuN+ and NeuN− from mouse cerebellum

(a) Area-proportional Venn diagram indicating intersections among CG-DMR-associated genes discovered by experiments using 10 or 0.5 ng NeuN+/NeuN− DNA and differentially expressed genes (DE, identified by mRNA-seq). (b) The level of CG methylation in non-CGI and CGI promoters plotted against mRNA rank in NeuN+ and NeuN−. Grey area represents s.e.m. n = 686 and 905 for non-CGI promoters in NeuN+ and NeuN−, respectively; 7107 and 7973 for CGI promoters in NeuN+ and NeuN−, respectively.

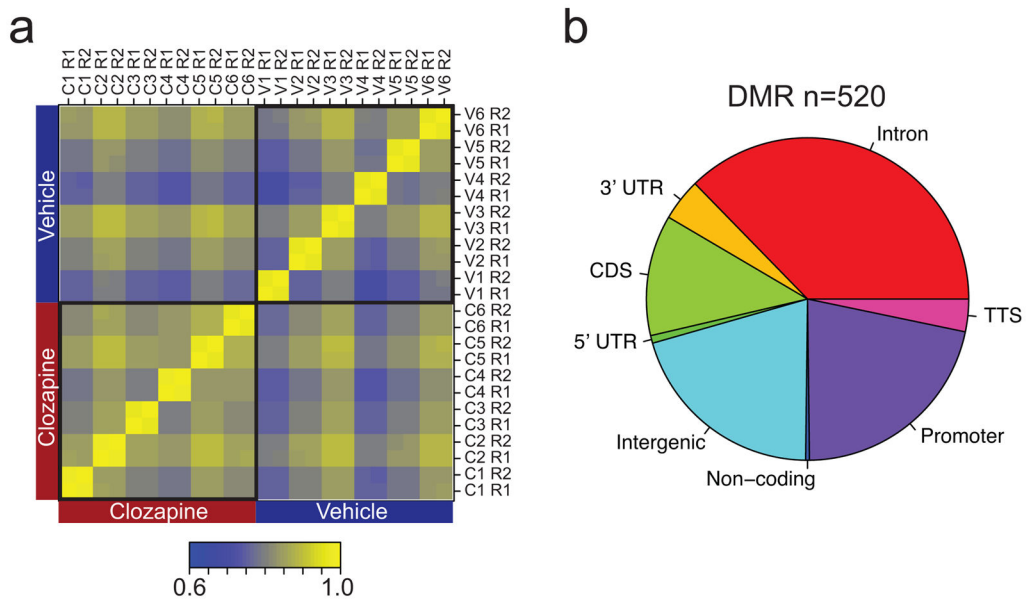

Figure 7. Methylomic changes in NeuN+ fraction from mouse frontal cortex associated with chronic clozapine treatment

(a) Pearson's correlations among various datasets. Each group of mice has 6 biological replicates (C1–6 for clozapine-treated mice and V1–6 for control mice injected with vehicle) and each sample had 2 technical replicates (R1 and R2, each obtained with 10 ng DNA). (b) The distribution of CG-DMRs (identified by comparing RRBS data take with C1–6 and V1–6) in various genomic features.